Positive frequency dependence of Q and geometrical spreading in crustal attenuation studies

Igor B. Morozov

Department of Geological Sciences, University of Saskatchewan, Saskatoon, SK S7N 5E2 Canada

Igor.Morozov@usask.ca

Abstract

Attenuation measurements by using crustal body, surface, or coda waves often result in frequency-dependent quality factor $Q \approx Q_0 f^{\eta}$ with $\eta > 0$. Such dependences can be explained as spurious and largely caused by variations of geometrical spreading (GS). In realistic lithospheric structures, GS is complex and often impossible or impractical to model. Nevertheless, GS variations can be measured concurrently with Q^{-1} and described by a parameter denoted γ. In body- and coda-wave measurements at 0 - 100-km observation distances, this parameter is consistently positive, which also causes positive η values. Here, the causes for such positive γ are examined by using 1D waveform synthetics. Generally, the results show that the upper-crustal structure and position of the earthquake hypocenter within it determine the character of GS. In typical crustal structures, γ is positive and of the order of 0.01 s^{-1}, in agreement with the observations. Strong velocity and attenuation contrasts within the upper crust and above the seismogenic zone further increase the values of γ in tectonically-active structures.

Key words: Geometric spreading; Seismic attenuation; Wave propagation.

1. Introduction

Frequency dependence of Earth-material quality factor (Q) is among the most intriguing subjects in seismology. Numerous arguments were advanced in favour of such frequency dependence based on theoretical, laboratory, and observational evidence (e.g., [1-6]). However, in this paper, I will not discuss these arguments but concentrate on only one specific question of whether and how the frequency-dependent $Q(f)$ can be measured in seismological data. Despite several decades of extensive studies, this basic question was still insufficiently addressed, apparently because of the already overwhelming preference for the $Q(f)$ concept. Seismological evidence for $Q(f)$ is often ambiguous because of its trade-off with geometrical spreading (GS), which is closely related to the difficulty of separating elastic-wave scattering from anelastic attenuation. Although this trade-off is well-known (e.g. [7]), it had not been extended to questioning the very existence of frequency-related variations of Q until I showed several examples [8-10] in which the entire measured frequency dependence of Q could be attributed to inaccurate GS. Additional recent examples are also given in [11,12], without a single exception so far in the frequency band from ~500 s to ~100 Hz. Many frequency-dependent $Q(f)$ models abundant in modern attenuation work are highly unconvincing, particularly those based on grossly inaccurate uniform-space GS corrections yet reporting strong increases of Q with frequency. To appreciate this concern, note that the end-member case of $Q \propto f$ is *completely indistinguishable* from a variation in GS and very low attenuation ($Q^{-1} = 0$), because the associated amplitude decay $\exp(-\pi f t/Q)$ is frequency-independent. Slower

than $Q \propto f$ decays may simply mean that some attenuation is also present, and faster-than f dependencies often found in coda studies (e.g., [13]) are completely meaningless, because they imply that scattering causes seismic waveforms to sharpen with propagation time. As shown in [8], "scattering Q" (Q_s) usually has strong observed frequency dependences [e.g., 17-21], can be explained by inaccurate GS.

As a first-order effect of the Earth's structure [e.g., 14], the GS should be nearly as variable as Q^{-1}, and therefore assuming a constant GS could be a bigger fallacy than regarding Q as frequency-independent. For example, Frankel et al. [22] pointed out that the effective GS of *S* waves in NE United States was significantly steeper than r^{-1}, where r was the hypocentral distance. From numerical modeling of that paper, one can also see that the GS does not follow any simple $r^{-\nu}$ dependence, but such an approximate dependence could be used within the distance range before the near-critical *SmS* reflection. Note that for *S* waves at epicentral distances $\Delta < 100$ km, the values of ν were consistently higher (~1.5 - 1.9) than the expected theoretical $\nu = 1$. For *Lg* waves ($\Delta =$ 100 - 400 km), ν equalled ~0.7, whereas it was postulated to equal 0.5 in the preceding frequency-domain studies [22].

When allowing a frequency-dependent Q in combination with variable GS, the attenuation-measurement problem becomes over-parameterized. For the three unknown parameters, such as Q^{-1}, $d(Q^{-1})/df$, and GS, only two constraints are typically available from attenuation measurements. For example, in most studies recovering the $Q^{-1}(f)$ values, such experimental constraints consist of the logarithm of the total seismic amplitude and its frequency derivative. In order to control the trade-off of the

attenuation-related parameters with GS, the latter is treated as fixed in most studies (e.g., [15,16]). However, although giving a conventional way for comparing the results, this solution to the trade-off problem is inadequate, because the resulting quantity denoted as "scattering Q" (Q_s) absorbs the errors of GS and leads to misleading descriptions of the lithospheric structure as randomly-scattering medium [9,23]. Moreover, when these medium parameters (including the GS [24,25]) are also regarded as frequency-dependent, this over-parameterization becomes overwhelming.

To resolve the GS – $Q(f)$ uncertainty, we have to realize the limits of information recoverable from the data and to apply physically reasonable simplifications in order to extract reliable parameters. Most importantly, trade-off should not be allowed in the physical properties of the medium, and consequently the Q, in its present form, cannot be such a parameter. However, I will use symbol "Q^{-1}" below in intuitive sense, to denote the "microscopic," random energy dissipation effects, by contrast to the GS related to larger-scale, deterministic Earth structure.

Realizing that GS is variable and unknown, let us now consider the following question: under what minimal conditions imposed on GS can it be separated from Q^{-1} effects empirically? Considering that the only source of data for such separation is essentially the frequency dependence of the attenuation coefficient, the answer to this question is that the GS variation can be separated from attenuation only by assuming that it is frequency-independent. This is a much weaker constraint than assuming a fixed GS, and this approach was taken in [8] and [11,12].

Not surprisingly, but maybe disappointingly for researchers interested in absorption-band type rheologies, all GS measurements performed to date [8, 11,12] led to

virtual elimination of the observed apparent $Q(f)$ dependences. Although considered as potentially frequency-dependent, the measured Q values became constant after only ~10% GS corrections in these studies. This estimate arises from considering the typical residual GS correction in the form of $e^{-\gamma t}$ [8], with $\gamma \approx 0.01$ s^{-1} in body- and coda-wave measurements (the definition of γ is given below). By equating this effect to an approximately equivalent $t^{-\delta\nu}$, we obtain $\delta\nu \approx \gamma t/\ln t$, which gives $\delta\nu \approx 0.09$ for a typical local-earthquake coda observation time of $t \approx 30$ s. With the background value of $\nu = 1$ [15], such GS variations should certainly be expected due to, for example, diving and reflected waves within a heterogeneous lithosphere.

In a worldwide compilation of short-period *S*-wave studies [8], the lithospheric GS was found to be systematically under-compensated by the standard t^{ν} corrections, with positive γ values ranging from ~0.002 to ~0.06 s^{-1}. Interestingly, γ values are also positive for *Lg* and Rayleigh waves at up to ~100-s periods, beyond which a slight negative γ is found [11]. For both body, coda, and Rayleigh waves, the values of γ are consistently increased in active tectonic structures, which was explained by the simplification and "homogenization" of the lithosphere with age [8, 11]. An increase of coda γ in more complexly-layered upper crust was suggested by numerical modeling in realistic lithospheric structures [27]. Note that unlike Mitchell [28], who suggested that the observed increase of crustal Q with tectonic age is related to the removal of fluids from the upper crust thereby decreasing its intrinsic attenuation, I interpret the increase of γ as a direct effect of changing crustal velocity profiles [29]. In addition, Q_i should also be low in the deformed, fractured, and "wet" young crust [11,28] and may increase with

age, although not so consistently as γ [8].

The systematically positive and age-related γ values appear extremely important for understanding attenuation observations, and their nature is not entirely clear. In this paper, I use numerical modeling of GS in several detailed velocity structures to provide explanation for such positive levels and to draw some conclusions about their possible origins. Because the apparent frequency-dependence parameter η is approximately proportional to γ [8], this should therefore also help explaining the observed predominance of positive η values in lithospheric-scale observations.

A secondary goal of this paper is to propose a simple form for the empirical GS law that is less "theoretical" and restrictive than the commonly used $G(t) = t^{-\nu}$ and could be more convenient for measuring the attenuation coefficient and inverted from the data. Our form is parameterized by the value of the attenuation coefficient at zero-frequency (γ) as $G(t) = t^{-\nu}e^{-\gamma t}$, where ν is the reference, conventional GS exponent, but γ should be measured from the data.

Numerical modeling

To examine the variability of geometrical effects within the lithosphere, I performed 1D waveform modeling in several 1-D crustal and upper mantle models. As in previous studies [27,30], synthetic seismic sections were created by using the reflectivity method [31]. The program by K. J. Sandmeier was modified to handle larger computations, parallelized, and incorporated in a seismic processing system [32] allowing seamless processing of the results.

Modeling resulted in over 800-s long, 3-component synthetic records sampled at 200-ms intervals and output at 1-km intervals from near-zero to 600-km distances from the epicentres. This allowed examining the wavefield to large offsets and avoiding any numerical wrap-around effects. The modelled frequency band was 0.2 - 2.4 Hz by using a "spike" source function suitable for spectral measurements. Sufficiently dense phase velocity spectrum from 1 to 120 km/s was selected in order to avoid frequency aliasing during numerical mode summations. As in any implementation of the propagator matrix method [33], all *P*/*SV* mode conversions and multiple reflections were accounted for in this modeling (Figure 1).

For each three-component record produced by the modeling, a sample-by sample root-mean square (RMS) trace was formed, and its peak vector amplitude and the total-trace energy were measured. The peak amplitudes were further squared, and both quantities multiplied by r^2 to correct for the reference r^{-1} GS of body waves. The amplitudes were finally scaled and presented together in Figures 2 - 4.

Several velocity models were tested, most of them based on the global IASP91 model [34] consisting of a simple three-layer crust and mantle without strong gradients and low-velocity zones (Figures 2 and 3). In order to focus on the geometrical effects, quality factors within the entire models were set large and equal $Q_P = 20000$ and $Q_S = 10000$. The densities were equal 2.8 g/cm^3 within the crust and 3.2 g/cm^3 within the mantle. In addition to the standard IASP91 model (Figure 2a), two of its modifications were also considered: one containing a 2-km thick low-velocity sedimentary layer with the same high *Q*'s (Figure 2b) and another one with strongly attenuating sediments: $Q_P = 20$ and $Q_S = 10$ (Figure 2c). Point sources were located at 7-km depths in all models.

Because of the crustal and mantle structure, the resulting wavefields are complex (Figure 1). Clearly, the "GS" represented by these sections is far from any of the theoretical "spreading-wavefront" models often employed in attenuation studies and contain abundant "multi-pathing" (i.e., reflections and mode conversions). Nevertheless, this amplitude pattern is much closer to those typically observed. This modeling shows that strictly speaking, GS cannot be associated with any particular seismic phase, but only with the time- or distance dependence of the wavefield. Note that although the free-surface, Moho and intra-crustal reflections cause rapid and persistent variations of the amplitudes recorded at the surface, distinct trends can be recognized in the pre-critical Moho reflection range (0 -100 km) and beyond it (Figures 2 - 4).

In all cases, the peak amplitudes (crosses in Figure 2, middle and bottom) show an approximately r^{-1} behaviour (near-horizontal slopes in Figure 2, middle and bottom), but only when averaged and considered beyond ~100-km distance ranges. Closer than ~60 - 70 km from the source, the amplitudes drop off quickly, corresponding to $\nu \approx 1.32$ for the IASP91 model and $\nu \approx 1.4$ - 1.5 for models with sedimentary layers (Figure 2). Around ~100-km hypocentral distances, near-critical Moho reflections arrive, whose GS-corrected amplitudes may rise above the level near the epicentre (in particular, for the IASP91 model, Figure 2a). At greater offsets, the *P*- and *S*-wave Moho reflections are followed by numerous multiples developing a more uniform GS (Figure 2, bottom).

An introduction of a sedimentary layer above the source increases the near-source GS exponent from $\nu \approx 1.3$ to 1.4 (Figure 2b). Such trend of increasing pre-critical ν was also observed in other models with heterogeneities located above the source. This effect was also noted by Frankel et al. [22], who explained it by waves reflecting downward

from the base of the sedimentary layer. The increased attenuation within the sediments appears to somewhat increase the spreading exponent to $\nu \approx 1.5$ (Figure 2c).

Notably, when additional reflectivity is placed below the source region, ν decreases and may drop below 1, and γ becomes negative (Figure 3). When the reflectors are located close beneath the source, the geometrically-compensated amplitudes rise monotonically from the source to about ~50 km (with $\nu \approx 0.93$), followed by a decay at larger offsets (Figure 3b). This behaviour resembles that observed in total-energy measurements [19], where such increased amplitudes were attributed to backscattering. This similarity is not surprising, as the reflectors below the source can indeed be viewed as "scatterers" returning the energy to the surface. However, "backscattering" is still a relatively loose term for these reflections, because it creates a connotation with random scattering in an otherwise uniform crust [18,20], whereas in reality we have predominantly upward reflections within a well-defined layered crustal structure. The distance dependence of these amplitudes should also be largely caused by wide-angle reflection coefficients varying with distance, and not by a $t^{-\nu}$-type GS. Also note that the position of the peak at ~50 km corresponds to the fixed source depth of 7 km in this modeling, and with deeper sources and reflective zone depths, the peak should accordingly move to longer offsets.

The two final numerical tests show a simple crustal model with a constant velocity gradient (Figure 4a) and a realistic platform model named "Quartz-4" and derived from detailed studies of Peaceful Nuclear Explosions (PNEs) in Russia [35] (Figure 4b). The model in Figure 4b was also used in our previous coda studies [27, 36]. As expected, in the gradient-crust model, the amplitude decay curves are the simplest and

show the best agreement with the theoretical r^{-1} dependence (Figure 4a). This is the only numerical example of good agreement with the assumed theoretical GS I have found so far. By contrast, because of its greater crustal thickness, the Quartz-4 model shows a range of amplitudes decaying faster than in any of the IASP91-based models, with $\nu \approx$ 1.7, followed by strong *PmP* and *SmS* onsets at ~150 km. Note that this large GS exponent is still within the range observed by Frankel et al . [22].

Interpretation of numerical results

To develop a model suitable for interpreting the above numerical, as well as experimental data, assume that there exists a "reference" Earth structure in which the GS, denoted $G_0(t, f)$, is close to the one observed. However, real structures (observed or modelled in a specific area), still differ from the reference one, and therefore seismic wave amplitudes should also be different. This difference may be caused by the variations in GS combined with the elastic and anelastic attenuation. In a perturbation- (scattering-) theory approximation [20], the deviation of the logarithm of the reference-GS compensated amplitudes is small and proportional to the propagation time t:

$$\ln\left(\frac{P(t, f)}{G_0(t, f)}\right) = -\chi(f)t\,, \tag{4}$$

where $\chi(f)$ is the attenuation coefficient and $P(t, f)$ is the path factor representing the observed amplitudes corrected for the source and receiver site effects [26]. In a different form, the path factor can be written as

$$P(t, f) = G_0(t, f)e^{-\chi(f)t}\,. \tag{5}$$

Further, by denoting the frequency-independent part of $\chi(f)$ by $\gamma = \chi(0)$, we can express $\chi(f)$ as

$$\chi(f) = \gamma + \kappa f \ . \tag{6}$$

Here, the second term vanishing at $f \to 0$ can be attributed to attenuation, and the frequency-independent term (γ) should be caused by the true GS. Considering the GS correction as frequency-independent, the true GS becomes

$$G(t, f) = G_0(t, f)e^{-\gamma t} \ . \tag{7}$$

Note that in this formula, $G_0(t,f)$, and therefore $G(t,f)$ may be frequency-dependent, but their ratio (residual GS) is frequency-independent. This is an important assumption without which it appears impossible to separate the effect of GS from Q^{-1}. However, note that by dropping the use of Q^{-1} and taking a consistently $\chi(f)$ approach [37], such separation may become unnecessary. The attenuation coefficient (6) can be best treated as a single quantity, and GS and a Q^{-1} not differentiated in modeling and interpretation.

The dimensionless parameter κ in eq. (6) can be attributed to the effective attenuation of the medium and also can be frequency-dependent. In [8], it was denoted as $\kappa = \pi/Q_e$ where Q_e was the "quality" parameter. Note that Q_e is defined so that its effect (i.e., term κf in eq. (6)) vanishes when no scattering or anelastic attenuation is present. Because of this property, Q_e does not trade-off with γ apart from the normal data-error covariance. By contrast, the conventional quality factor $Q(f) = \pi f/\chi(f)$ [16] spuriously, linearly increases with frequency when no attenuation is present but GS is inaccurately corrected for: $Q(f) = \pi f/\gamma$ when $\kappa = 0$. When $\gamma < 0$, $Q(f)$ can even become negative.

The exponential form of $P(t, f)$ in eq. (5) leads to a straightforward measurement procedure for γ and Q_e by using logarithms of spectral ratios, as illustrated in [8-10,27,30, 37]. Parameter γ is obtained from the intercepts of the $\chi(f)$ dependences at $f = 0$, and Q_e is measured from their slopes. If the $\chi(f)$ dependence shows significant deviations from linearity in f, a frequency-dependent Q_e can be derived from its curvature.

GS varies for different wave types and frequency bands, and therefore we use the conventional $G_0(t, f) = t^{-\nu}$ approximation, in which ν is selected differently for the different frequency bands and types of observations. In our body-wave examples (Figures 2 - 4), ν is considered equal 1, and γ represents the corresponding variations of GS. The relatively small values of γ (Figures 2 - 4, bottom) show that this approximation is acceptable within the ~0 - 100-km distance ranges. For other types of waves, ν can be different (such as ½ or 0.83 for *Lg* [38]) and γ would vary accordingly. Therefore, γ may also vary with frequency bands, offset ranges, and observations using different types of $G_0(t, f)$ (for more on this, see [27,11]). Also, for refracted body waves (*Pn* or *Sn* [24,25]) and in fact for any realistic "coloured" reflection sequence, $G_0(t, f)$ is inherently frequency-dependent. However, this does not alter the role of γ as the measure of GS deviations from its best-known reference level.

In the synthetic data (Figures 2 - 4), parameter γ was measured from our synthetic data shown in bottom plots in by using the following relation (see eq. 4):

$$\left\langle \ln\left[E(t, f)t^2\right]\right\rangle_f = \left\langle 2\ln\left[\frac{P(t, f)}{G_0(t, f)}\right]\right\rangle_f = const - 2\gamma t . \qquad (8)$$

Angular brackets $\langle\ldots\rangle_f$ here denote the averaging of the frequency-dependence in our

time-domain measurements. This frequency dependence is dominated by the source spectrum produced by the numerical simulator combined with the "coloured" response of the structure mentioned above. Therefore, the γ values measured here represent averages of the frequency-dependent GS:

$$\gamma_{\text{measured}} = \left\langle \chi(f)\big|_{Q^{-1}=0} \right\rangle_f \tag{9}$$

and not exactly the values of $\chi(0)$ defined in eq. (6). However, we ignore this frequency-dependence of GS here and only emphasize the leading term in γ.

Similarly to the exponential form, the time dependences (8) of the reference-GS corrected amplitudes can be alternately approximated by a $t^{-\delta\nu}$ function, from which:

$$\left\langle \ln\left[E(t, f)t^2\right] \right\rangle_f = const - 2\delta\nu \ln t\,, \tag{10}$$

where $\delta\nu$ is the residual GS exponent. The corrected values of $\nu = 1 + \delta\nu$ are also shown in Figures 2 - 4. Note that dependence (10) can only be fit beyond ~5-km offsets, apparently where the reflections from the free surface become significant (middle-row plots in Figures 2 - 4). This shows that the $t^{-\nu}$ law represents a poorer approximation for the actual GS whereas dependence (8) covers the modeled GS well from 0 to ~50 - 100-km distances (Figures 2 - 4). This should be due to the perturbation type, $t^{-\nu}e^{-\gamma t}$ GS law not distorting the t^{-1}-type spreading in the immediate vicinity of the source.

Discussion

In different types of attenuation measurements (e.g., body-wave, *Lg*, coda, or total-energy), different seismic phases and time windows are selected for measuring the

amplitudes leading to eq. (5). The peak and averaged whole-record amplitudes shown in Figures 2 - 4 are likely most relevant to *P*-wave, coda, and total-energy studies. However, my goal here was not to model any specific case with sufficient accuracy, which may not always be possible. Instead, the goals were to demonstrate that the GS generally: 1) is measurable and can be modeled by waveform synthetics to some extent, 2) does not fit into any simple models such as $t^{-\nu}$, 3) is variable and sensitive to the lithospheric structure. In particular, these numerical experiments show that because of the upper-crustal reflectivity, GS is *commonly faster* than expected from an isotropic, uniform-space t^{-1} model. These conclusions are practically invariant in respect to the choices of time windows and types of amplitude measures.

In addition to the simplified GS law, note that association of a specific window (such as the ~3.5-km/s window commonly selected in *Lg* measurements) represents another conventional simplification affecting the seismic amplitudes measured in the data or synthetics. However, with carefully selected windows and crustal models matching the observation environments, modeling results should still likely bear some common features.

Such common features appear to be as follows. For most crustal models without strong mid-upper crustal reflectivity (such as in Figures 2 and 4), the numerical modeling showed values of $\gamma > 0$. Such structures are likely to be most abundant around the world, and therefore the GS should most often be under-compensated by the standard body-wave correction r^1. In the traditional attenuation measurements based on transforming $\chi(f)$ into $Q(f) = \pi f/\chi(f) = \pi f/(\gamma+\kappa f)$ and then taking $Q(f) = Q_0 f^{\eta}$, positive γ values lead to $\eta > 0$. As shown in [8], parameter η can be approximated as $\eta \approx \pi\gamma/(f_{obs}Q_e)$, where f_{obs} is

the central observation frequency. Therefore, the fact of $\gamma > 0$ explains widespread observations of positive and high η's, especially for lower f_{obs}, and in higher-γ, lower-Q_e settings. Note that both of these last conditions correspond to tectonically-active areas [8].

The predicted values of γ range from -0.005 to ~0.01 s^{-1} (Figures 2 - 4), and similar values were also derived from numerous observations [8]. To ascertain whether such residual GS levels should be significant in attenuation measurements, let us define a reference level γ_Q so that its effect equals that of the effective attenuation, that is $\gamma_Q = \pi f_{obs}/Q_e$. With typical values of $Q_e \approx 1000$ and $f_{obs} \approx 1$ Hz, $\gamma_Q \approx 0.003$ s^{-1}, which is below most of the modelled and observed γ values (Figures 2 - 4; [8,11]) Therefore, in most cases, the residual GS should affect the measurements of Q. As a simple rule, the larger the value of η is, the more significant is the effect of γ [8].

Interestingly, the level of $\gamma \approx 0.008$ s^{-1} derived for model Quartz-4 (Figure 4b) is close to the measurements from real *Lg* coda data in this PNE and also to independent numerical coda simulations, from which $\gamma \approx 0.0075$ s^{-1} [27]. This suggests that scattered body waves at 0 - 100 km distances make key contributions to the coda. Also, from a worldwide compilation of *S*- and *Lg*-wave results, the same level of $\gamma_D \approx 0.008$ s^{-1} represents the threshold separating tectonically active ($\gamma > \gamma_D$) and stable ($\gamma < \gamma_D$) regions [8]. This shows that parameter γ correctly captures an important common factor differentiating these lithospheric structures; it appears that this common factor could likely be the GS.

Upper-crustal reflectors above the hypocenter deflect the upcoming waves and

cause steeper GS (Figures 2b, c). Modeled γ values increase when sedimentary layers are present above the hypocenter, and particularly when these layers have lower intrinsic Q (compare Figure 3 to 2). This suggests a potential explanation to the observed trend for γ decreasing with tectonic age [8]. Tectonically young structures are more likely to have strong velocity and attenuation contrasts within the upper crust and above the seismogenic zone [29]. Due to cooling, metamorphism, and dehydration, such contrasts erode with age, leading to decreasing γ. Note that a uniform pressure-related crustal velocity gradient has no significant GS effect (Figure 4a). Therefore the upper-crustal structure is the most important for causing increased levels of γ.

The upper-crustal reflectivity also appears to be the only suitable mechanism for reducing γ and particularly for obtaining GS-compensated amplitudes that increase away from the hypocenter (i.e., $\gamma < 0$). To produce such increasing amplitudes, reflective layers should be present close and below the source (Figure 3b). Such reflectors enhance the illumination of the pre-critical distance interval for Moho reflections.

Notably, in all cases considered above, the total-energy GS differs from that of the peak-amplitude. The total-energy curves show much faster amplitude decays to ~200-km distances compared to the peak amplitudes (grey diamonds and black crosses, respectively, in Figures 2 - 4). A significant portion of the energy appears to be removed from the direct waves in the vicinity of the source and propagates as faster-dissipating, probably surface-wave modes. Although this effect could be insignificant in body-wave attenuation studies using only the highest-amplitude direct arrivals, such difference should be important in total-energy and coda studies, where the entire wavefield

contributes to the measurements. Therefore, in coda attenuation studies, neither of the empirical GS curves in Figures 2 - 4 should be sufficiently accurate (not to mention the theoretical $r^{-\nu}$ dependences), and special modeling needs to be conducted [27].

The above observations show that the upper-crustal structure and position of the earthquake source within it are definitely the most important factors forming GS patterns. The GS, in its turn, controls the results of most $Q(f)$ measurements. Therefore, it appears that the only two reasonable approaches to the assessment of the true frequency dependence of Q are:

1) Develop and accurate GS correction by comprehensive numerical modeling of the lithospheric structures in the study area;

2) Seek Q measurement approaches not relying on GS compensation, such as the attenuation-coefficient or spectral ratio methods.

Unfortunately, approach 1) would always be prone of uncertainties related to the lack of knowledge of the structure, source mechanisms, instrumental, and site effects. The three-dimensional structure along the propagation paths will hardly be ever known to the detail required for sufficiently accurate modeling independently of Q^{-1} (i.e., without any knowledge about scattering and attenuation!) and by using the complete wavefield. Although very important for verification of hypotheses and interpretation, when used as the basis for observations, modeling could again land us in a quagmire of assumptions and biases embedded in the measurements. Therefore, after even the best-possible modeling is conducted, it should be verified and corrected by approach 2).

The empirical approach 2) is by far more reliable and adequate for describing the

data. Its strength is in utilizing the fundamental property of attenuation as energy dissipation process related to the frequency of wave oscillations. One problem with this approach is that spectral amplitude data typically show large scatters that only rarely allow determination of a frequency-dependent Q_e. For example, no indications of frequency-dependent Q_e were found so far in several studies revisited by using this technique [8,9,11]. Nevertheless, physical theories should recognize the limitations of the data, and perhaps frequency-independent Q_e is all we can have at the moment. Also, the observed frequency independence of Q_e represents a much stronger constraint on the physics of wave propagation within the Earth, indicating that relaxation-mechanism rheology and scattering are not nearly as pervasive within the crust and mantle as it is thought today. With ever increasing volumes and quality of seismological data, the potential frequency dependence of Q_e should undoubtedly become measurable in the future.

Waveform simulations of this study indicate that γ is sensitive to the position of the earthquake source within the lithosphere. For sources located below the zone of upper-crustal reflectivity, the modelled GS tends to be systematically faster than theoretical, with $\gamma \approx 10^{-3} - 10^{-2}$ s^{-1}, which is in agreement with the observations [8]. The heterogeneous upper crust deflects the source energy downward. Note that this effect could be attributed to "scattering attenuation" and described by parameter Q_s; however, such attenuation is neither random nor isotropic as implied by this name [9,23].

Both γ modelled in this study and its corresponding Q_e are "apparent" parameters representing the observations of GS and attenuation on the surface. Clearly, for complex structures considered here, their inversion for the in-situ properties of the lithosphere is a

non-trivial task related to "reversing" the waveform modeling above. However, two general observations about the in-situ properties can already be made from these results. First, because of the similarity between γ and Q^{-1} comprising a single attenuation coefficient $\chi(f)$, it appears that the solution could be sought in the form of the corresponding "intrinsic attenuation coefficient" $\chi_i(f) = \gamma_i + \pi f/Q_i$ associated with points within the medium. This suggests using attenuation tomography to invert for both γ_i and Q_i. Second, because of the same similarity, it appears that frequency-independent Q_e should normally result (i.e., unless special additional constraints are imposed) in frequency-independent intrinsic Q_i models. Thus, combined with observations [8,11], modeling described here reinforces our confidence that a frequency-independent intrinsic Q should be sufficient for describing the existing seismological observations. However, these indications yet remain to be corroborated by detailed inversions.

Finally, in applied studies such as nuclear-test monitoring, $Q(f)$ is often viewed more as a wave amplitude (e.g., coda shape) parameter than a property related to a well-defined physical process, and the ambiguity of the assumed GS is less consequential (W. S. Phillips, personal communication). Nevertheless, in such studies, the final interpretation is still often carried out by correlating Q_0 and η to regions and geological structures, by relating them to tectonic types and crustal temperatures, and by transporting these parameters into similar regions. However, as Q_0 and η also trade-off with the unknown and variable GS, they cannot be uniquely compared to geology. By contrast, the results of [8,27] and of this paper show that stable and improved interpretations should result from using the γ and Q_e parameters, which can be measured from the data and predicted by numerical simulations.

Conclusions

Waveform numerical modeling in lithospheric structures shows that geometrical spreading (GS) of seismic waves should be complex and regionally variable, and thus impossible to represent by using a fixed theoretical dependence on the distance, as it is commonly done in attenuation studies. After the traditional GS-compensation, residual variations in GS lead to spurious frequency dependence of the attenuation quality factor Q.

Because of its irresolvable trade-off with the GS, the elastic attenuation factor Q_s is interpreted as a theoretical artefact, and therefore its use should be avoided in data inversions. Instead of this parameter, I suggest using γ in the semi-empirical GS law in the form of $G(t) = t^{-\nu}e^{-\gamma t}$. Modeling shows that this parameter correctly describes the variations of GS within the distance range below the critical Moho reflection onsets (0 - 100 km). From the perturbation-theory point of view, γ also represents the zero-frequency limit of the generalized scattering coefficient: $\gamma = \chi(f=0)$.

In most synthetic models examined, positive values of γ were found, indicating stronger GS compared to the commonly used theoretical predictions. This could explain positive frequency dependences ($\eta > 0$) of the apparent $Q(f)$ observed in many areas and attenuation studies.

The upper-crustal structure and the position of the hypocenter within it determine the character of GS. Reflectors above the earthquake hypocenter tend to increase γ, and reflectors immediately below the source – to decrease it. With sufficiently strong reflectivity below the source, γ may become negative and lead to geometrically-

compensated amplitude peaks at 30 - 70-km hypocentral distances, which are also often attributed to Q_s. Such sensitivity of GS to the upper-crustal structure may explain the inferred decrease of γ with tectonic age [8].

Acknowledgements

This research was supported by NNSA Grant DE-FC52-05NA26609 and also in part by NSERC Discovery Grant RGPIN261610-03.

References

1. Knopoff, L., "*Q*," *Reviews of Geophysics*, vol. 2, no. 4, pp. 625-660, 1964.

2. Jackson, D.D., and D. L. Anderson, "Physical mechanisms of seismic-wave attenuation," *Reviews Geophysics and Space Phys*ics, vol. 8, no. 1, pp. 1-63, 1970.

3. Liu, H. P., D. L. Anderson, and H. Kanamori, "Velocity dispersion due to anelasticity: implications for seismology and mantle composition," *Geophysical Journal of Royal Astronomical Society*, vol. 47, pp. 41–58, 1976.

4. Anderson, D. L, and J. W.Given, "Absorption band *Q* model for the Earth," *Journal of Geophysical Research,* vol. 87, pp. 3893-3904, 1982.

5. Doornbos, D. J., "Observable effects of the seismic absorption band in the Earth," *Geophysical Journal of the Royal Astronomical Society*, vol. 75, pp. 693-711, 1983.

6. Sato, H., and M. Fehler, "Seismic wave propagation and scattering in the heterogeneous Earth," Springer-Verlag, New York, 308pp, 1998.

7. Kinoshita, S., "Frequency-dependent attenuation of shear waves in the crust of the southern Kanto area, Japan," *Bulletin of the Seismological Society of America*, vol. 84, pp. 1387-1396, 1994.

8. Morozov, I. B., "Geometrical attenuation, frequency dependence of *Q*, and the absorption band problem," *Geophysical Journal Int*ernational, vol. 175, pp. 239-252, 2008.

9. Morozov I.B., "Thirty years of confusion around "scattering *Q*"?," Seismological Research Letters, vol. 80, pp. 5-7, 2009

10. Morozov, I.B., "Earth's Structure as the cause of frequency-dependent t^* and Q," AGU Fall Meeting, San Francisco, CA, Dec 14-18, 2009, paper S41B-1914, 2009.

11. Morozov I.B., "Attenuation coefficients of Rayleigh and *Lg* waves," *Journal of Seismology*, in review.

12. Morozov I. B., "On the causes of frequency-dependent apparent seismological *Q,"* *Pure and Applied Geophysics*, in review

13. Hazarika, D., S. Baruah, and N. K. Gogoi, "Attenuation of coda waves in the Northeastern Region of India," *Journal of Seismology*, vol. 13, pp.141–160, DOI 10.1007/s10950-008-9132-0, 2009.

14. Banda, E.., N. Deichmann, L., W. Braile, and J. B Ansorge, "Amplitude study of the *Pg* phase," *Journal of Geophysics*, 51, 153-164, 1982.

15. Aki, K., "Scattering and attenuation of shear waves in the lithosphere," *Journal of Geophysical Research,* vol. 85, pp. 6496-6504, 1980.

16. Aki, K. and B. Chouet, "Origin of coda waves: source, attenuation, and scattering effects," *Journal of Geophysical Research,* vol. 80, pp. 3322-3342, 1975.

17. Dainty, A. M., "A scattering model to explain seismic *Q* observations in the lithosphere between 1 and 30 Hz," *Geophysical Research Lett*ers, vol. 8, pp. 1126-1128, 1981.

18. Wu, R.-S., "Multiple scattering and energy transfer of seismic waves, separation of scattering effect from intrinsic attenuation," *Geophysical Journal of the Royal Astronomical Society,* vol**.** 82, pp. 57-80, 1985.

19. Toksöz, M. N., A. M. Dainty, E. Reiter, and R.-S. Wu, 1988. "A model for attenuation and scattering in the earth's crust," *Pure and Applied Geophysics*, pp. 128, 81-100, 1988

20. Jin, A., K. Mayeda, D. Adams, and K. Aki, "Separation of intrinsic and scattering attenuation in southern California using TERRAscope data," *Journal of Geophysical Research,* vol. 99, pp. 17835-17848, 1994.

21. Mayeda, K., F. Su, and K. Aki, "Seismic albedo from the total seismic energy dependence on hypocentral distance in southern California," *Physics of the Earth and Planetary Interiors*, vol. 67, pp. 104-114, 1991.

22. Frankel, A., A. McGarr, J. Bicknell, J. Mori, L. Seeber, and E. Cranswick, "Attenuation of high-frequency shear waves in the crust: measurements from New York State, South Africa, and southern California, " *Journal of Geophysical Research,* vol. 95, pp. 17441-17457, 1990.

23. Morozov I. B., "Reply to "Comment on 'Thirty Years of Confusion around 'Scattering *Q*'?'" by J. Xie and M. Fehler," *Seismological Research Letters*, vol. 80, pp. 637-638, 2009

24. Yang, X., T. Lay, X.-B. Xie, and M. S. Thorne M.S., "Geometric spreading of *Pn* and *Sn* in a spherical Earth model," *Bulletin of the Seismological Society of America*, vol. 97, pp 2053–2065, doi: 10.1785/0120070031, 2007.

25. Zhu, T., K.-Y. Chun, and G. F. West, "Geometrical spreading and *Q* of *Pn* waves: an investigative study in western Canada," *Bulletin of the Seismological Society of America*, vol. 81, pp. 882-896, 1991.

20. Chernov, L.A., "*Wave Propagation in a Random Medium*," McGraw-Hill, New York, 168pp., 1960.

26. Fan, G.-W. and T. Lay, "Strong *Lg* attenuation in the Tibetan Plateau," *Bulletin of the Seismological Society of America,* 93, pp. 2264-2272, 2003.

27. Morozov, I. B., C. Zhang, J. N. Duenow, E.A. Morozova, and S. Smithson, "Frequency dependence of regional coda *Q*: Part I. Numerical modeling and an example from Peaceful Nuclear Explosions," *Bulletin of the Seismological Society of America*, vol. 98, pp. 2615–2628, doi: 10.1785/0120080037, 2008.

28. Mitchell, B. J., "Anelastic structure and evolution of the continental crust and upper mantle from seismic surface wave attenuation," *Reviews of Geophysics*, vol. 33, pp. 441-462, 1995.

29. Christensen, N. I., and W. D. Mooney, "Seismic velocity structure and composition of the continental crust: A global view," *Journal of Geophysical Res*earch, vol. 100, no. B7, pp. 9761-9788, 1995.

30. Morozov, I. B., "Crustal scattering and some artifacts in receiver function images", *Bulletin of the Seismological Society of America*, vol. 94, pp. 1492-1499, 2004.

31. Fuchs, K., and G. Müller. "Computation of synthetic seismograms with the reflectivity method and comparison with observations," *Geophysical Journal of Royal Astronomical Society*. vol. **23**, 1971.

32. Chubak, G., and Morozov, I. B., 2006. "Integrated software framework for processing of geophysical data," *Computers & Geosciences*, vol. 32, pp. 767-775, 2006.

33. Aki, K., and P. G. Richards, "*Quantitative Seismology*," Second Edition, University Science Books, Sausalito, CA, 2002.

34. Kennett, B.L.N. and R. Engdahl, "Traveltimes for global earthquake location and phase identification," *Geophysical Journal* International, vol. 105, pp. 429-465, 1991.

35. Morozova, E.A., I. B. Morozov, S. B. Smithson, and L. N. Solodilov, "Heterogeneity of the uppermost mantle beneath Russian Eurasia from the ultra-long range profile QUARTZ," *Journal of Geophysical Research*, vol. 104, pp. 20329-20348, 1999.

36. Morozov, I. B. and S. B. Smithson, S. B., "Coda of long-range arrivals from nuclear explosions," *Bulletin of the Seismological Society of America*, vol. 90, pp. 929-939, 2000.

37. Morozov, I. B., "On the use of quality factor in seismology," *AGU Fall Meeting*, San Francisco, CA, Dec 14-18, 2009, paper S44A-02, 2009.

38. Campillo, M., 1990. "Propagation and attenuation characteristics of the crustal phase *Lg*," *Pure and Applied Geophysics*, vol. 132, pp. 1-17.

Figures

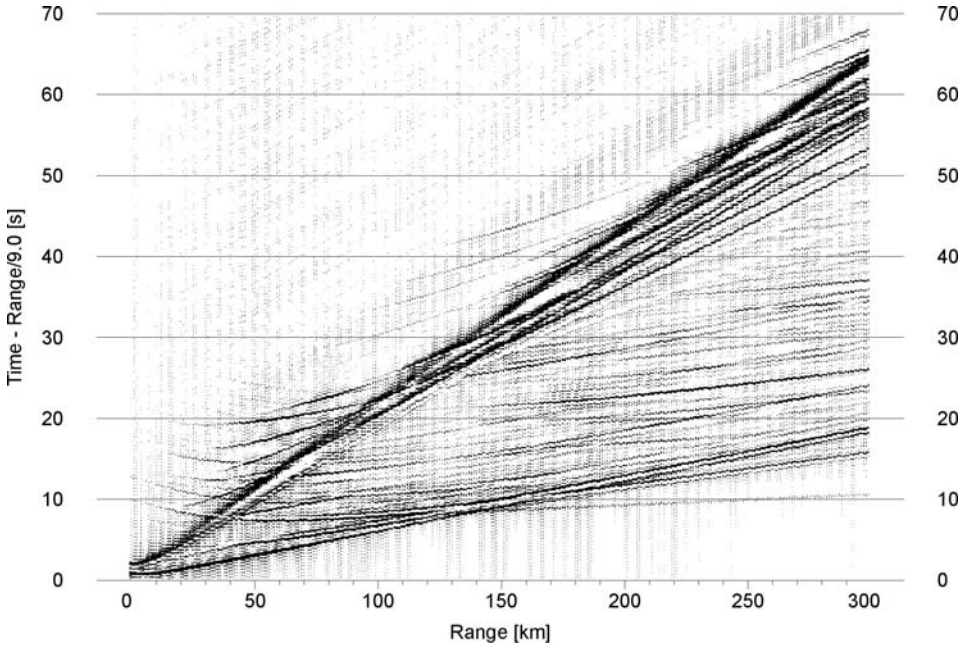

Figure 1. Vertical-component synthetic record section modeled in IASP91 lithospheric structure. Travel-time reduction velocity of 9 km/s was used for plotting. Note the complex wavefield which is interpreted as representing the "geometrical spreading."

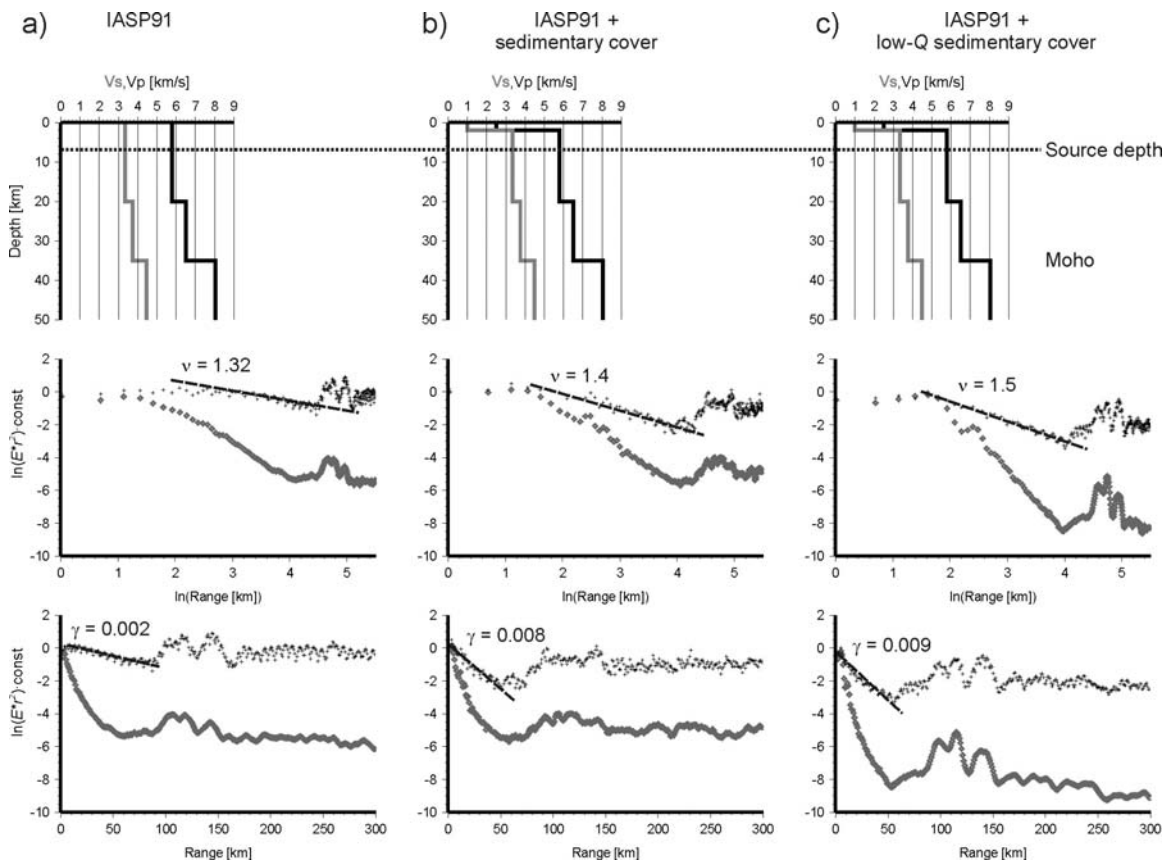

Figure 2. Results of numerical simulations in: a) IASP91 model, b) IASP91 with low-velocity sedimentary layer, c) the same as b) but with $Q_P = 20$ and $Q_S = 10$ within the sedimentary layer. *Top row*: the V_P and V_S velocity models; *Middle row*: geometrical spreading within near-offset ranges, in logarithmic distance scale; *Bottom row*: the complete distance range in linear scale. Grey diamonds show the total recorded energy and black crosses – peak energy in two (radial and vertical) components combined. Both amplitudes are geometrically-compensated by using the theoretical $(range)^2$ factor. Dashed lines labelled with ν values indicate the approximations of geometrical spreading using the $t^{-\nu}$ law at near offsets, and lines with labels γ show the same ranges approximated by $e^{-\gamma t}$ dependences.

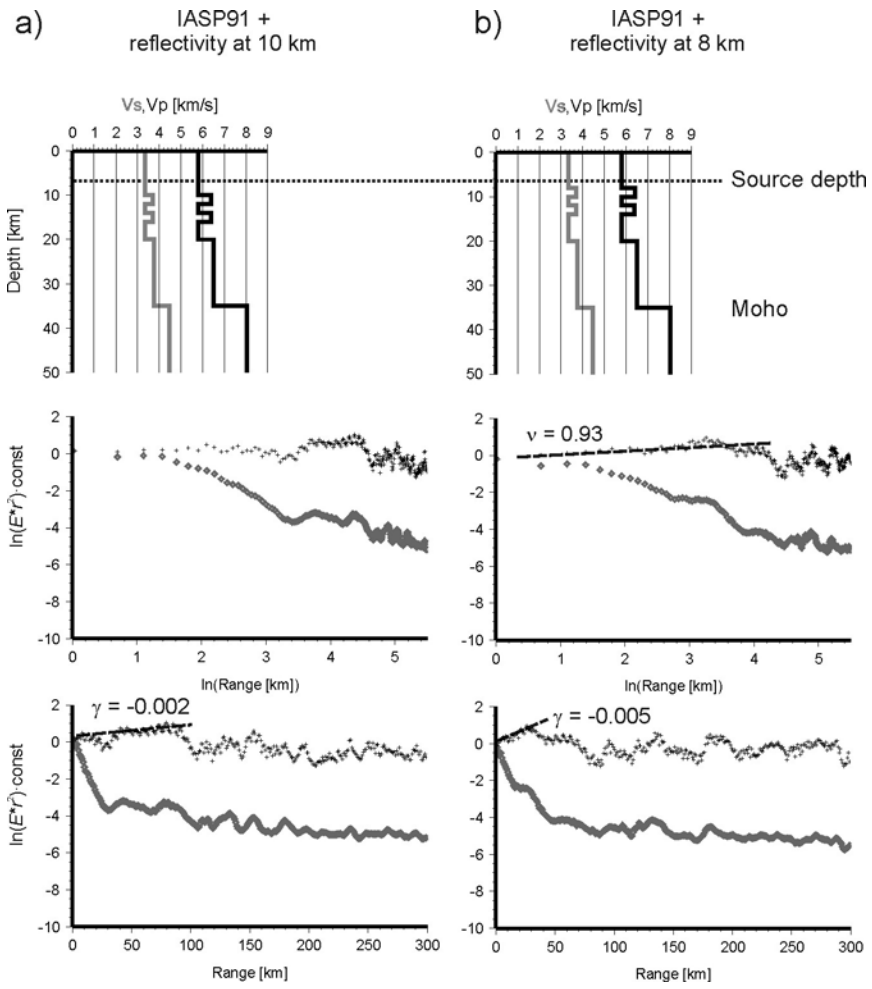

Figure 3. Modeling results with a reflectivity zone below the source at 7 km: a) reflectivity starting at 10-km depth, b) starting at 8-km depth. Geometrical compensation, lines, and labels are as in Figure 2. Note the slower geometrical spreading at near offsets (ν and γ) dropping below the theoretical level of $\nu = 1$ and $\gamma = 0$ in case b).

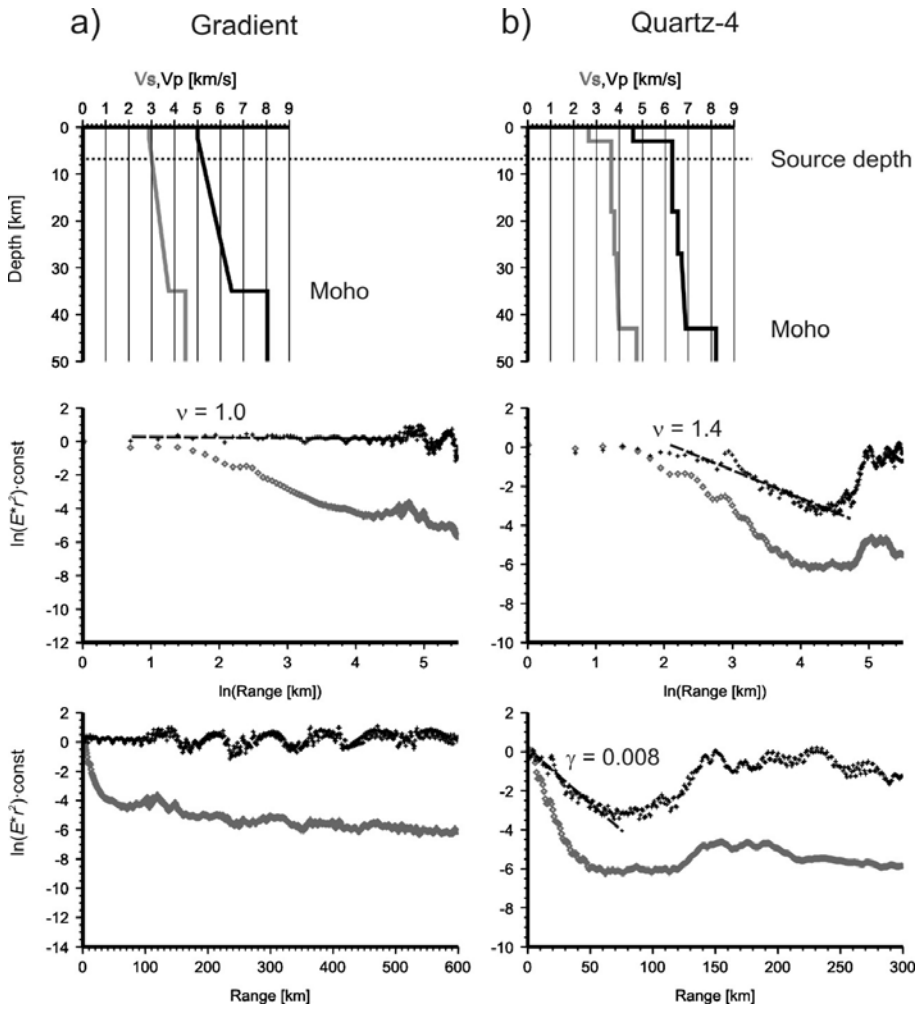

Figure 4. Modeling results for: a) a hypothetical gradient model of the crust; b) detailed, realistic structure from inversion PNE Quartz-4 in Russia [35]. Geometrical compensation of the amplitudes, lines and labels as in Figure 2.